Design and experiment of the traction tiger nut combine harvester

Wenhui Chen[1,2,3], Jiaming Fei[1,2,3], Jianping Gao[1,2,3], Za Kan[1,2,3], Lidong Huang[4], Hewei Meng[1,3*], Jiangtao Qi[1,2*]

(1. *College of Mechanical and Electrical Engineering, Shihezi University, Shihezi 832000, Xinjiang, China*;
2. *Engineering Research Center for Production Mechanization of Oasis Characteristic Cash Crop, Ministry of Education, Shihezi 832000, Xinjiang, China*;
3. *Key Laboratory of Northwest Agricultural Equipment, Ministry of Agriculture and Rural Affairs, Shihezi 832000, Xinjiang, China*;
4. *Guilin Maike Machinery Co., Ltd, Guilin 541000, Guangxi, China*)

Abstract: The conventional tiger nuts harvesting method suffers from several drawbacks, including low harvesting efficiency, high levels of impurities, significant loss rates, and excessive labor intensity. To address these issues, a novel operational approach of sand removal first and then separatingwas introduced. A tractor-mounted tiger nuts combine harvester was designed to perform the tasks of excavation, sand removal, and rhizome separation of tiger nut tubers in a single operation. The machine's overall structure and operational principles are described. It then details the design of critical components, such as the combined vibration digging device, the conveying and sand removal device, the cylinder screening device, and the wind-screen cleaning device. The structural and dynamic parameters of these key components were established through an analysis of the mechanism's motion and the material flow during the combined vibration digging, conveying sand removal, cylinder screening, and wind-screen cleaning processes. Field trials demonstrated the harvester achieved an average loss rate of 4.88%, the average impurity rate (excluding gravel content) of 7.52%, and an average digging depth of ≥12.5 cm. Throughout the testing phase, the machine operated reliably, and the results fulfilled the operational requirements for the tiger nut harvester.

Keywords: tiger nuts, combined vibration digging device, conveying and sand removal device, cylinder screening device, wind-screen cleaning device
DOI: 10.25165/j.ijabe.20261902.9681

Citation: Chen W H, Fei J M, Gao J P, Kan Z, Huang L D, Meng H W, et al. Design and experiment of the traction tiger nut combine harvester. Int J Agric & Biol Eng, 2026; 19(2): 139–151.

1 Introduction

Tiger nuts, also known as Cyperus esculentus, belong to the sedge family, and have the reputation of "underground walnut" They are widely distributed in Africa, Spain, North America, and China[1]. Their underground tubers are rich in protein, fiber, fat, and carbohydrates[2,3], and the oil yield is as high as 25%, which is two times that of peanuts and four times that of rapeseed[4-6]. Due to its high oil yield, tiger nuts are widely expected to be a substitute for soybeans to alleviate the growing domestic demand for oil. However, tiger nuts grow underground. During the harvest process, tiger nuts are mixed with rhizomes and sandy soil, which is more complicated. Most of the existing tiger nut harvesters in China are improved from potato and other tuber harvesters[7]. Due to the poor matching effect of machine structure and working parameters, the efficiency of the tiger nut harvesting process is low, and the loss rate and impurity rate are high. It is difficult to meet the requirements of mechanized harvesting of tiger nuts. Therefore, it is necessary to develop an efficient tiger nut combine harvester to make up for the shortage of tiger nut mechanical harvesting and promote the development of tiger nut-related industries.

In recent years, domestic and foreign scholars have carried out a lot of research on the harvesting technology and equipment of tiger nuts. In the research of tiger nuts, Qu et al.[8] developed a self-propelled tiger nut harvester. Dong et al.[9] designed a traction tiger nut harvester. Liu et al.[10,11] designed a composite tiger nut harvester equipped with separating and cleaning components, enabling sand-soil separation, bean root threshing, and effective tiger nut harvesting. However, with the increase of feeding amount, the working efficiency and separation effect decrease. The cutting and throwing process of the digging device to the soil is the main factor causing the high-power consumption of the whole machine[12]. The Shangshuqi team of Qingdao Agricultural University designed a reverse rotary-type tiger nut digging device[13,14]. With the help of the discrete element method, the tool movement, structural parameters, and working characteristics were analyzed. It was found that reverse rotary digging can reduce the digging resistance. Zhang et al.[15] and Pei et al.[16] found that the use of vibration excavation can effectively reduce the excavation resistance, and the digging rate and damage rate are significantly improved. These research results provide an important reference for optimizing the digging device and reducing the power consumption of the whole machine.

As the main working part of the tiger nut combine harvester, the conveying and separating parts are widely used in the harvesting

Received date: 2025-01-13 **Accepted date:** 2026-02-09
Biographies: Wenhui Chen, PhD candidate, research interest: agriculture machinery, Email: 20242309204@stu.shzu.edu.cn; **Jiaming Fei**, PhD candidate, research interest: agriculture machinery, Email: feijm9812@163.com; **Jianping Gao**, PhD candidate, research interest: agriculture machinery, Email: 20232009048@stu.shzu.edu.cn; **Za Kan**, Professor, research interest: agriculture machinery, Email: kz_mac@shzu.edu.cn; **Lidong Huang**, Engineer, research interest: agriculture machinery, Email: 1211268343@qq.com
***Corresponding author: Hewei Meng**, PhD, Professor, research interest: agriculture machinery. College of Mechanical and Electrical Engineering, Shihezi University, Shihezi 832000, Xinjiang, China. Tel: +86-13369935035, Email: mhw_mac@shzu.edu.cn; **Jiangtao Qi**, PhD, Associate Professor, research interest: agriculture machinery. Engineering Research Center for Production Mechanization of Oasis Characteristic Cash Crop, Shihezi 832000, Xinjiang, China. Tel: +86-15699322648, Email: qjtjd@shzu.edu.cn.

operation of related rhizome crops. Wang et al.[17] established a dynamic model for the transport and separation process of Panax notoginseng root-soil complex, analyzed the operation mechanism of the transport and separation device, and optimized the transport and separation performance. Zhao et al.[18] designed a scraper-type sassafras bean conveying device. Xin et al.[19] established a dynamic model of potato conveying and separation system, and analyzed it by the progressive method, which improved the separation efficiency of potato and soil and ensured the quality of harvest. Chen et al.[20] constructed a multi-body dynamics simulation model of vibrating potato-soil separation device based on DEM-MBD. It shows that providing appropriate vibration is an effective method to improve the separation rate of potato-soil. The above research involves the separation of soil and fruit. However, due to the particularity of small size and irregular shape of tiger nuts, the above conveying and separating device cannot be directly used, but it can provide reference for the design of a tiger nut conveying and separating device. Based on the EDEM-MBD simulation method, Zhang et al.[21] studied the influence of structural parameters and motion parameters on the screening performance of the double-layer cylinder screen fruit and impurity separation device. The results show that the cylinder screen is suitable for the threshing and separation of tiger nuts, and the separation performance can be greatly improved with the cleaning components. However, the separation performance gradually decreases under the condition of long-term large feeding by using the cylinder separation component to realize sand-soil separation and bean root threshing, which needs further optimization.

In conclusion, to address the issues of low harvesting efficiency, high impurity rate, and high loss rate in the tiger nut harvesting process, this paper introduces an operation mode of removing sand first and then separating. Additionally, a tiger nut combine harvester is designed, which integrates components such as vibration digging, conveying and sand removal, cylinder screening, and wind-screen cleaning. Through a detailed analysis of the structural, dynamic, and kinematic characteristics of the key working parts, the overall working performance of the combine harvester is revealed. The objective of this study is to develop a combined harvester suitable for the sandy areas of Xinjiang, thereby providing valuable insights for the advancement and utilization of mechanized harvesting technology and equipment for tiger nuts in this region.

2 Basic structure and working principle

2.1 The whole structure and technical parameters

The tiger nut combine harvester is mainly composed of a depth limiting device, combined vibration excavation device, conveying and sand removal device, double-layer drum screening device, air-screen cleaning device, lifting device, and walking device. The excavation operation of the harvester is completed by the depth limiting device and the combined excavation device. The conveying and sand removal device completes the sand removal operation, and the separation operation is completed by the drum separation device and the air-screen cleaning device. Its structure and main technical parameters are shown in Figure 1 and Table 1.

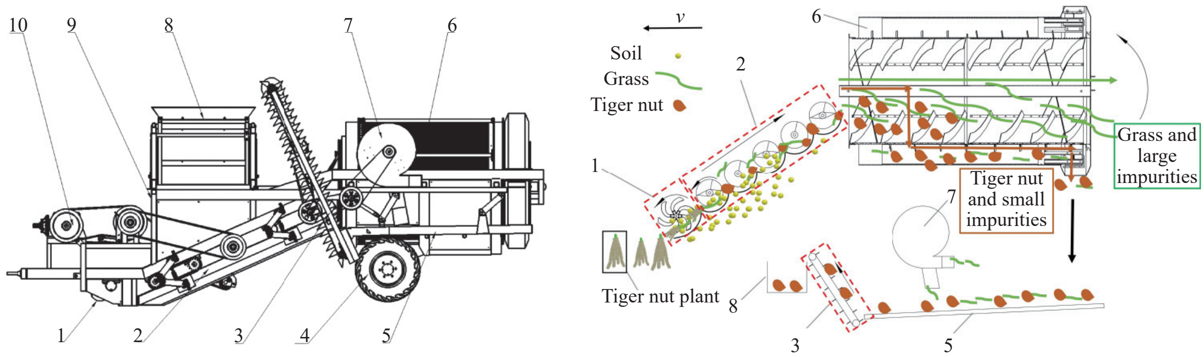

a. Schematic of the harvester structure b. Schematic of the harvester working principle

1. Combined vibration digging device 2. Conveying and sand removal device 3. Bucket lifting device 4. Walk device 5. Screen body 6. Cylinder screening device 7. Fan 8. Collecting box 9. Frame 10. Gear box

Note: v is the forward operating speed of the harvester.

Figure 1 Structure diagram of tiger nut harvester

Table 1 Main technical parameters of tiger nut combine harvester

Parameter	Numerical value
Length × Width × Height/mm×mm×mm	4900×2600×1600
Distance between wheels/mm	1700
Working width/mm	1600
Working speed/km·h^{-1}	0.5-1.5
Digging depth/mm	150-200
Walking manners	Traction type

2.2 Working principle

The schematic of the tiger nut harvester working principle is shown in Figure 1b. When the tiger nut harvester is working in the field, the tiger nuts-root-sand complex is dug out from the sand soil under the action of the combined vibration excavation device and scattered and thrown to the conveying and sand removal device. At this time, the mixture of tiger nuts, root, sandy soil, and grass are transported to the double-layer drum screening device along the ‘S’ route under the action of multi-stage winch and vibrating screen, and the sand removal is realized at the same time. The tiger nuts and root are threshed under the action of the rotating strike of the flow-assisted spiral blade and the drum screen. Large impurities such as rhizomes are transported to the grass discharge outlet. Tiger nuts and small impurities enter the outer sieve through the inner sieve hole and enter the air sieve cleaning device through the discharge outlet. The stratification is facilitated by the movement of the vibrating screen, and the light impurities are removed under the action of the negative pressure fan. The tiger nut seeds enter the lifting device and are transported to the granary with the lifting device. The remaining impurities are discharged from the machine to complete the tiger nut harvesting operation.

3 Key parts design

3.1 Structure design of combined vibration digging device

The digging device is a direct contact soil component. Its main function is to completely dig out, break up, and transport the tiger nuts-rhizome-sand soil complex, which is mainly composed of rotary blade, digging shovel, and so on. The structure diagram is shown in Figure 2. The preliminary test results of the project team show that sand accounts for more than 95% of the mixture of beans, roots, and sand excavated at the time of harvest[22]. When mechanized harvesting operations are carried out, it is necessary to carry out sand cutting operations. It is also necessary to break and transport the bean-root-sand complex, which has problems such as high energy consumption and large wear. Therefore, a combination of rotary tillage excavation and vibration excavation is proposed for excavation operations.

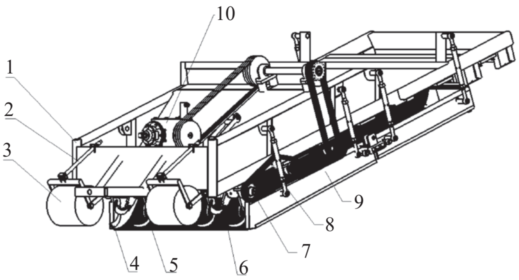

1. Frame 2. Depth limit wheel adjustment mechanism 3. Depth limit wheel 4. Rotary blade 5. Vibration digging shovel 6. Rotary blade axis 7. Transmission system 8. Vibration digging shovel connecting rod 9. Screen body 10. Gear box

Figure 2 Structure diagram of combined vibration digging device

3.1.1 Design of rotary blade

As one of the key components of the digging device, the rotary blade throws the tiger nuts-root-sand complex backward while crushing and cutting sand. Combined with the growth depth and operation requirements of tiger nuts, it is determined that the digging depth needs to reach 15 cm. Therefore, a curved rotary blade with throwing effect and large tillage depth is selected.

The power consumption of the rotary tillage digging device is mainly the power consumption of the rotary blade. According to the empirical transmission mode, the sprocket transmission is adopted. Before the sprocket selection, the power consumption should be calculated first. According to the previous test, the overall power consumption of the tiger nut vibration digging device is about 15 kW, and the calculated power P_c of the sprocket is

$$P_c = \frac{K_A K_Z}{K_m} P \tag{1}$$

where, K_A is the working condition coefficient, taking 1.5; K_Z is the tooth number coefficient. Considering that it is a sealed sprocket that goes deep into the ground and needs to reduce the size, the tooth number of the pinion is 15 and the tooth number coefficient is 1.8; K_m is the multi-row chain coefficient, taking 1.0; P is the transmitted power, kW.

The calculated power P_C = 40.5 kW of the sprocket of the tiger nut vibration digging device can be obtained by bringing the data into Equation (1). At the same time, combined with the research status of the existing tiger nut vibration digging devices at home and abroad, the applicable speed range of the tiger nut vibration digging device should be 300-450 r/min, and the device has complex operation conditions. Therefore, to meet the vibration digging test, the maximum speed of all components of the device is 450 r/min. Therefore, the 16A sprocket group is selected as the transmission part of the device.

3.1.2 Design of vibration digging shovel

The digging shovel is divided into fixed digging shovel and vibration digging shovel in form. The fixed digging shovel harvesting technology equipment generally has the problems of large digging resistance and high power consumption, while the vibration digging shovel can effectively reduce the digging resistance and reduce the power consumption, thereby improving the operation efficiency[23]. The vibration digging shovel designed in this paper has digging shovel, cam, roller, and so on. The digging shovel is welded at the front end of the vibrating screen of the conveying sand removal device, and the roller is installed on the vibrating screen. At the same time, the cam is installed on the shaft of the horizontal screw conveyor. When the sprocket group works, it will drive the horizontal screw conveyor and the rotary blade shaft to rotate. The cam impacts the roller to promote the reciprocating vibration of the vibrating screen. The schematic diagram of the digging shovel structure is shown in Figure 3. The vibration digging shovel is attached under the frame. Except for a section of the front blade of the vibration digging shovel (vibration digging flat shovel), the rest of the shovel surface is made into a fine grid strip shape (vibration grid strip sieve) to complete the separation of some sand and soil, which can reduce some resistance and power consumption. The two ends of the shovel surface are connected with the shell of the rear material conveying part.

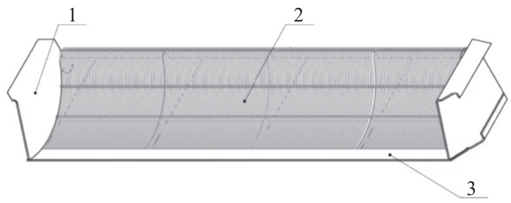

1. Baffle plate 2. Grid screen 3. Shovel blade

Figure 3 Structure diagram of vibration digging shovel

The length, width, and inclination of the blade of the digging shovel will affect the digging resistance and power consumption. The inclination of the shovel surface should not only overcome the digging resistance, but also make the digging shovel have good self-cleaning function to ensure that the rising objects of the shovel surface can leave the shovel smoothly[24]. The smaller the inclination angle of the shovel surface is, the higher the cutting efficiency is, and the forward resistance decreases, but the situation of broken soil becomes worse. At the same time, the inclination angle is too small, and the wear resistance of the shovel tip decreases. When the inclination angle of the shovel surface increases, the forward resistance gradually increases, and the power consumption increases[25]. The previous team measured that the friction angle between the sand and the digging shovel was 17°, and the friction angle between the tiger nuts and the digging shovel was 22°. According to the Agricultural Machinery Design Manual[26], the inclination angle of the shovel surface should be less than 24°. Therefore, the inclination angle of the shovel surface is taken as $\gamma = 20°$. Through the preliminary test, the optimal working width of the whole machine is 1600 mm. Therefore, the designed shovel length is slightly larger than the working width, taking 1650 mm. The total longitudinal width of the shovel is 370 mm, the height of the shovel is 169 mm, the width of the vibrating digging flat shovel is 100 mm, the radius of the vibrating grid sieve is 300 mm, and the gap of the grid is 6 mm.

The structural principle of the vibration digging shovel is shown in Figure 4. In the figure, the cam is installed on the E point and the roller is installed on the F point, and the two points are in contact. At the same time, the length of the connecting rod of the two vibration digging shovels before and after is equal, that is, $BC = AD$; N is any point on the vibration shovel.

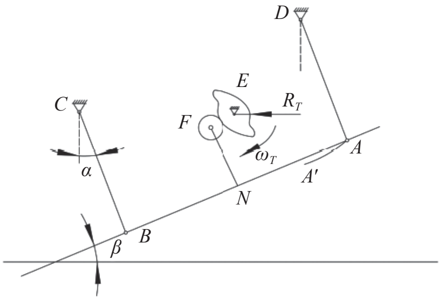

Note: R_T is cam radius, mm; ω_T is the angular velocity of the cam, rad/s; β is the vibration digging shovel and horizontal angle, (°); α is the hanging angle of the connecting rod, (°).

Figure 4 Structural schematic diagram of vibration digging shovel

The vibration device is composed of cam, roller, and so on. The front and back of the vibration digging shovel are hinged with the rack through two equal length connecting rods. The rotation of the cam produces an exciting effect on the roller, which drives the front and back vibration of the digging shovel installed at the front end of the vibrating screen. At the same time, the vibration shovel also swings up and down at the hinged point of the connecting rod and the rack. The digging shovel, the connecting rod, and the rack form a parallel four-bar mechanism. The whole vibration shovel can be approximately regarded as a simple harmonic motion in the forward direction and the vertical forward direction. Therefore, the displacement, velocity, and acceleration of the N point on the vibration shovel can be obtained.

$$S_T = (H_T - R_T)|\sin(\omega_T t)| \tag{2}$$

$$V_T = \omega_T (H_T - R_T)|\cos(\omega_T t)| \tag{3}$$

$$a_T = -\omega_T^2 (H_T - R_T)|\sin(\omega_T t)| \tag{4}$$

Where, S_T is the displacement of point N on the vibration shovel, mm; V_T is the velocity of point N on the vibration shovel, m/s; a_T is the acceleration of point N on the vibration shovel, m/s²; H_T is the distance from the cam crown to the center of the circle, mm; t is the movement time, s.

When the device moves forward at speed, the absolute motion trajectory of point N (as a point on the tip of the shovel) on the fixed coordinate will be projected in the X and Y directions, which is expressed as:

$$\begin{cases} X_N = v_m t + (H_T - R_T)|\sin(\omega_T t)| \cdot \cos\alpha \\ Y_N = (H_T - R_T)|\sin(\omega_T t)| \cdot \sin\alpha \end{cases} \tag{5}$$

Eliminating the time parameter t from Equation (5) will obtain

$$X_N = \frac{\arcsin\left(\left|\dfrac{Y_N}{(H_T - R_T)\cdot\sin\alpha}\right|\right)}{\omega_T} + Y_N \cot\alpha \tag{6}$$

The slope of any point on the trajectory curve represents the velocity direction of the point. When some structural parameters are not reasonably selected, the bottom surface of the vibration shovel and the sand will have a strong impact in the work, so that the whole machine cannot continue to work. Therefore, if it is required that the bottom surface of the shovel does not collide with the bottom sand at this point, it is necessary to ensure that the angle between the velocity direction of the point and the horizontal plane is less than the horizontal inclination angle of the shovel.

So, according to Figure 4 and Equation (6), the following equation can be obtained:

$$\omega_T \leq \frac{v_m \tan\beta}{(H_T - R_T)(\sin\alpha - \tan\beta\cos\alpha)} \tag{7}$$

It is known that the moving speed of the machine is 0.1-0.4 m/s. At this time, the horizontal inclination angle of the vibration digging shovel is considered to be 0°-15°. According to Equations (6) and (7), the amplitude of the vibration digging shovel is 6-12 mm and the vibration frequency is 10-15 Hz.

3.2 Structure design of conveying and sand removal device

The rotary blade cuts the sand into pieces and then throws it to the circular arc vibrating screen. The conveying and sand removal device composed of multi-stage horizontal screw conveyors is used to transport the tiger nuts mixture to the drum-type separation device, and the sand is removed during the transportation process. The device is composed of a multi-stage horizontal screw conveyor, an arc-type vibrating screen, an excitation device, etc., and the auger of the adjacent horizontal screw conveyor rotates in the opposite direction. The tiger nuts mixture is transported on the arc-type vibrating screen in the ‘S’ route, which increases the effective screening time and improves the screening efficiency. The structure diagram of the device is shown in Figure 5.

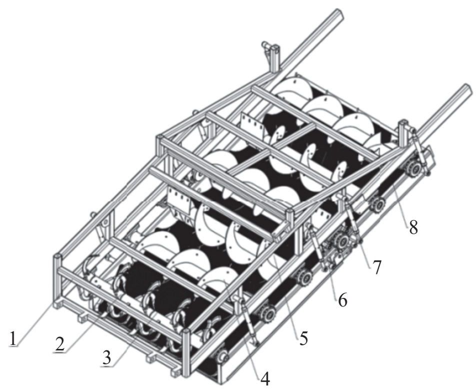

1. Frame 2. Combined vibration excavation device 3. Front screen body 4. Screw conveying device 5. Rotary blade 6. Vibration device 7. Vibrating screen connecting rod 8. Back-end screen body

Figure 5 Structure diagram of conveying and sand removal device

When working, to ensure that the material moves in the ‘S’ route in the device, the horizontal screw conveyor adopts the winch structure to transport the material axially, and the scraper is installed at the end of the winch to realize the backward transportation of the material, as shown in Figure 6.

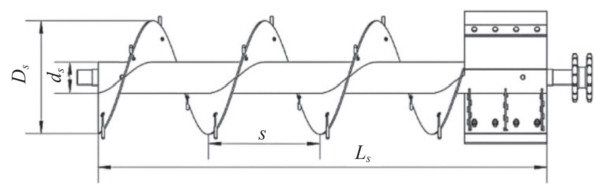

Note: L_s is the horizontal screw conveyor, mm; D_s is the diameter of the spiral blade, mm; s is the screw distance, mm; d_s is the diameter of the screw shaft, mm.

Figure 6 Structure diagram of screw conveying device

Conveying capacity is an important index to measure the productivity of the horizontal screw conveyor[26].

$$Q = 47D_s^2\varphi Cs\gamma n \tag{8}$$

where, Q is the amount of material transported, t/h; γ is the proportion of material accumulation, t/m^3; φ is the filling factor, taking 0.3; K is the empirical coefficient of the comprehensive characteristics of the material, taking 0.06; C is the correction coefficient of inclined conveying, because the conveying angle is 0°, taking $C = 1$; n is the rotational speed of screw shaft, r/min.

The diameter of the spiral blade directly affects the conveying capacity of the conveyor[27].

$$D_s = K\sqrt[2.5]{\frac{Q}{\varphi\gamma C}} \tag{9}$$

The rotation speed of the screw shaft is an important parameter affecting the conveying efficiency of the horizontal screw conveyor, which can be calculated according to the following Equation (10).

$$n_1 \leq \frac{A}{\sqrt{D_s}} \tag{10}$$

where, n_1 is the maximum allowable speed of the screw shaft, r/min; A is the comprehensive characteristic coefficient of material.

The diameter of the spiral blade is calculated to be $D_s \approx$ 0.402 m, and the whole is D_s = 400 mm; horizontal screw conveyor pitch S = (0.9 to 1.5)D_s = 400 mm; the inner diameter of the horizontal screw conveyor is d_s =(0.2 to 0.35)D_s =108 mm. Considering the installation space of the horizontal screw conveyor, the shaft length of the horizontal screw conveyor is L_s = 1600 mm.

The power consumption of the conveying and sand removal device is mainly the power consumption of the horizontal screw conveyor rotating and driving the vibration of the vibrating screen. According to the empirical transmission mode, the sprocket transmission is used to calculate the required power consumption. Because the excitation source of the vibrating screen is installed on the spiral shaft, it is calculated according to the spiral conveyor. The power of the screw conveyor is determined by the resistance generated during the movement, including the friction resistance of the material to the spiral surface, the gravity component resistance generated during the axial transportation of the material, and the additional resistance generated by the stirring and crushing during the material migration. The power of the screw shaft can be expressed by the following Equation (11).

$$N_0 = k_1\frac{Q}{367}\omega_0 L \tag{11}$$

where, N_0 is the power required for the rotating shaft, kW; k_1 is the power reserve coefficient; Q is productivity, t/h; ω_0 is the total resistance coefficient of material; L is the horizontal projection length of screw conveyor, m.

Previous studies have found that[28] the power of the whole conveying sand removal device is about 33 KW. When the amplitude of the vibrating screen is 4.7 mm and the vibration frequency is 7.5 Hz, the sand removal efficiency can reach 88.92%. At the same time, it is found in the study that the rotational speed of the spiral conveyor at all levels affects the axial and backward conveying speed of the sand-soil mixture, and the conveying speed has a great influence on the sand removal effect. Therefore, the maximum speed of the screw shaft is determined to be 340 r/min, and the 16 A sprocket group is selected for the supporting power transmission.

3.3 Structure design of cylinder screening device

The separation device is a key component that determines the operation quality of the harvester and determines the operation performance of the whole machine. In the previous study, it was found that the threshing of tiger nuts was relatively easy, and the sand and soil were basically removed by the conveying and sand removal device. Most of the tiger nuts, rhizomes, and a small amount of sand and soil mixture entered the separation device. Therefore, the cylinder screening device was selected to further realize the threshing and separation of tiger nuts and impurities. The assembly structure of the cylinder screening device is shown in Figure 7. The cylinder screening device adopts a cylindrical double-layer screen, and the inner wall is equipped with a flow-assisted spiral blade. The operation is driven by the central shaft. The inner screen realizes the separation of tiger nuts from large impurities such as rhizomes, and the outer screen realizes the separation of tiger nuts from smaller impurities. One end of the drum screen is connected to the discharge end of the desilting device, and the other end is the discharge port and the grass discharge port. The cylinder screening device is installed on the frame through the support wheel.

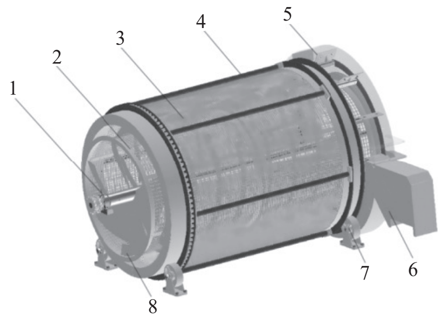

1. Separating screw conveyor 2. Inner roller screen 3. Outer roller screen 4. Vertical support rod 5. Lifting scraper 6. Discharging opening 7. Support wheel 8. Flow-supporting spiral blade

Figure 7 Structure diagram of cylinder screening device

3.3.1 Cylinder screen diameter and length

The diameter and length of the cylinder screen directly affect the screening effect and the ability to treat tiger nuts extracted per unit time[29]. Regarding the cylinder screen, a larger drum diameter typically leads to better screening performance. However, an overly large diameter can result in a bulky structure, cumbersome movement, and significant vibration. Taking into account the working width and installation space of the entire machine, the inner diameter of the inner screen is set at D_1 = 1.0 m. The diameter D_2 of the outer cylinder screen is calculated based on empirical Equation (12)[26].

$$D_2 = \left[\frac{11.36Q_m}{Fk_2g^{0.5}\tan\alpha}\right]^{0.4} \times 0.037\,808 \tag{12}$$

where, Q_m is the maximum feeding amount of the drum, m^3/s; F is the filling coefficient, generally taking 0.25-0.33; k_2 is the velocity correction factor, taking 1.0; g is acceleration of gravity, taking 9.8 m/s^2; α is the inclination angle of the cylinder screen, (°).

According to the actual operation, the maximum feeding amount Q_m = 33 m^3/h, and the outer cylinder screen diameter $D_2 \approx$ 1.4 m can be calculated by Equation (12).

The length of the cylinder screen will affect the screening performance of the drum screen. To avoid the decrease of the working efficiency of the whole machine caused by the low screening efficiency, it is necessary to meet[26]:

$$\begin{cases} q_s S \geq Q(1-\sigma) \\ S = \pi DL \end{cases} \tag{13}$$

where, q_s is the sieve unit area which can bear the screening material quality, taking 2.5 kg/s·m^2; σ is the mass ratio of impurities in tiger nut, taking 0.21; D is the diameter of the cylinder, m; L is the length of the cylinder screen, m; Q is the feeding amount of cylinder screen, kg/s; S is the screen area, m^2.

According to experience, the length of the cylinder screen is generally two to six times its diameter. Considering the installation space of the roller screen and the matching with the whole machine, the length of the roller screen is taken as two times the diameter.

$$2D_1 \leq L \leq 2D_2 \tag{14}$$

That is, 2.0 m $\leq L \leq$ 2.8 m; combined with the spatial layout of the whole machine, the length of the cylinder screen is taken as L = 2.3 m.

3.3.2 Screen selection and sieve design

The screen type directly affects the screening effect. The types of sieve commonly used in agriculture mainly include punching sieves, grid sieves, and fish-scale sieves. Among them, the preparation sieve has high opening rate, light weight, and convenient installation, so the preparation sieve is selected. The common sieve shapes are circular, square, triangular, and long circular holes. In this paper, the sieve is rectangular. The screening quality of the material per unit area of the screen is related to the utilization coefficient of the screen surface. When the shape of the screen is fixed, its size is related to the size, arrangement, and spacing of the screen holes[30]. In the case of other relevant parameters being unchanged, the greater the utilization coefficient of the sieve surface, the higher the screening efficiency and the better the screening effect. The sieve surface utilization coefficient K_0 is

$$K_0 = \frac{b^2}{(b+d)^2} \times 100\% \tag{15}$$

where, b is the clear width of the sieve, mm; d is the diameter of sieve wire, mm.

The sieve size of the inner and outer layers of the sieve mesh should be determined according to the triaxial size of tiger nuts. Because the shape of tiger nut seeds is oblate, the triaxial sizes of tiger nuts are 6.85-10.4, 8.09-14.77, and 5.96-9.74 mm. Considering that there are impurities such as rhizomes in the extract of tiger nuts entering the drum sieve, the screening function of the inner and outer sieves is different. If the size of the inner sieve is too large, it will lead to too many rhizomes entering the outer sieve, affecting the screening performance of the outer sieve. If the outer sieve hole is too large, the loss rate increases. If the sieve hole is too small, it is easy to cause blockage. In the case of ensuring the stiffness and strength of the screen body, the larger the screen hole width, the higher the utilization coefficient of the screen surface, and the better the screening effect. Therefore, the diameter of the sieve bar is 3 mm, the sieve hole of the inner screen is square, the width is 25 mm, the sieve hole of the outer screen is rectangular, the length is 30 mm, the width is 6 mm, and the utilization coefficient of the inner screen surface is 76.95% calculated by Equation (15).

3.3.3 Analysis of material movement in cylinder screen

The screening effect is determined by the motion state of the material in the cylinder screen, and the rotational speed of the cylinder screen is an important parameter affecting the separation effect of the extracted tiger nuts. The material migration state in the screen is also different with different rotational speeds. The rotational speed of the inner cylinder screen should be between the maximum rotational speed and the minimum rotational speed. The maximum rotational speed is that the material moves to the highest point with the drum screen, and the centrifugal force is equal to the rotational speed of gravity. The minimum rotation speed is the rotation speed when the material moves to the horizontal position of the center of the drum screen, and the friction force generated by the centrifugal force at the screen hole is equal to the gravity[31]. Without considering the center axis and the interaction force between the materials, the material is regarded as a particle. The material in the cylinder screen is mainly affected by gravity G, friction f, centrifugal force F_1, and support force F_n. The cross section is selected on the vertical axis of the cylinder screen, and the Cartesian coordinate system is established along the center line of the cylinder screen. The circular motion of the material with the rotation of the cylinder screen is analyzed, as shown in Figure 8.

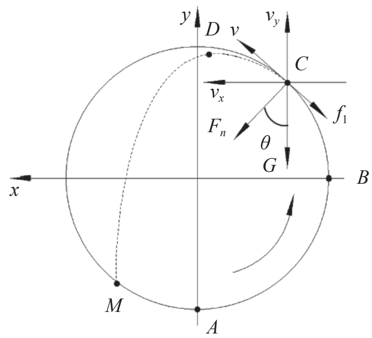

Note: A is the lowest point of the drum; B is the edge point of the drum in the horizontal direction; C is the detachment point, where the material leaves the cylinder wall to start the projectile motion; D is the highest point of the trajectory of the material projectile; M is the falling point after the material falls; v is the linear velocity of the material at the moment of C point detachment, m/s; v_x and v_y are the components of the material detachment velocity in the x-axis and y-axis directions, respectively, m/s; θ is the angle between the screen support force F_n and the gravity G of the material, (°).

Figure 8 Force analysis of material in cylinder screen

The force of the material along the y axis in the arc BD section is as follows:

$$\begin{cases} F_n = F_1 - G\cos\theta \\ G = mg \\ F_1 = m\omega^2 R \\ \omega = 2\pi n/60 \end{cases} \tag{16}$$

where, R is the radius of the cylinder screen, taking 0.5 m; ω is the angular velocity of the cylinder screen, rad/s; n is the rotation speed of the cylinder screen, r/min; m is the material quality in the sieve, g; θ is the angle between the screen support force F_n and the gravity G of the material, (°).

When the cylinder screen speed is low, the material rises to a certain height along the screen surface under the friction of the cylinder screen, and the fluidity of the material in the screen is not good, which is not conducive to screening. With the increase of the rotational speed of the cylinder screen, the material can be transported to the arc BC section. At this time, the material is subjected to gravity greater than centrifugal force, and the material leaves the screen surface to make a waterfall movement, so that the material moves repeatedly from the inner layer to the outer layer. At this time, the material has good fluidity, which is conducive to particle screening, and the screening effect is remarkable. When the rotational speed continues to increase, the material can migrate to the highest point. At this time, the material is subjected to centrifugal force, which can completely offset its own gravity. Under the action of centrifugal force, the material is close to the screen, the material fluidity is poor, and the screening loss rate increases.

In summary, after the material is lifted to point C, the waterfall movement occurs. At this time, the centrifugal force of the material is equal to the resultant force of the gravity along the y-axis and the support force of the sieve surface. When the material moves to point D, the support force of the sieve surface to the material is zero, and the angle between the gravity direction and the support force is zero.

The conditions for the waterfall movement of the sieve surface material are

$$G\cos\theta \geq F_1 \tag{17}$$

Available from above,

$$n \leq \frac{30}{\pi}\sqrt{\frac{g\cos\theta}{R}} \tag{18}$$

It can be calculated that n≤33.4 r/min. Considering the actual operation needs, the rotation speed of the cylinder screen is n= 25 r/min.

As shown in Figure 8, the material moves with the drum screen to C and then leaves the screen surface to do the waterfall motion, which is composed of two parts: the CD segment oblique throwing motion and the DM segment falling motion. Ignoring the interaction between the tubers and the interaction between the tubers and the impurities, the material waterfall motion is analyzed.

When the material is about to be separated from the sieve surface, the centripetal force acting on the material is

$$F = F_N + mg\cos\theta \tag{19}$$

The velocity along the x and y axes at point C is

$$\begin{cases} v_{Cx} = 2\pi nR\cos\theta \\ v_{Cy} = 2\pi nR\sin\theta \end{cases} \tag{20}$$

In the fall movement, the material is affected by gravity and air resistance, and the air resistance is

$$f_1 = -k_3 v \tag{21}$$

where, f_1 is air resistance, N; k_3 is the coefficient of air resistance; v is the initial velocity of the dropping motion, m/s.

The oblique throwing speed after the material is separated from the screen surface is analyzed.

$$\begin{cases} m\dfrac{\mathrm{d}v_{Cx}}{\mathrm{d}t} = -f_1\cos\theta \\ m\dfrac{\mathrm{d}v_{Cy}}{\mathrm{d}t} = -f_1\sin\theta - mg \end{cases} \tag{22}$$

Equation (23) can be obtained by the integral of Equation (22).

$$\begin{cases} v_x = v_{Cx}\mathrm{e}^{-\frac{k_3 t}{m}} \\ v_y = \mathrm{e}^{\frac{k_3 t}{m}}\left(v_{Cx} + \dfrac{mg}{k_3}\right) - \dfrac{mg}{k_3} \end{cases} \tag{23}$$

After the material is removed from the screen surface, it moves to the highest point D. At this time, $v_y = 0$, and the oblique throwing time t_1 can be obtained.

$$t_1 = \frac{k_3}{m}\ln\left(\frac{mg}{k_3 v_{Cy} + mg}\right) \tag{24}$$

The displacement along x and y axes at any time can be obtained.

$$\begin{cases} L_x = \displaystyle\int_0^t v_x \mathrm{d}t \\ L_y = \displaystyle\int_0^t v_y \mathrm{d}t \end{cases} \tag{25}$$

The coordinates of point D can be obtained by bringing $t = t_1$ into Equation (25).

$$\begin{cases} L_{xD} = -\dfrac{k_3}{m}v_{Cx}\mathrm{e}^{-\frac{k_3 t_1}{m}} \\ L_{yD} = \mathrm{e}^{\frac{k_3 t_1}{m}}\left(v_{Cx} + \dfrac{mg}{k_3}\right)\dfrac{k_3}{m} - \dfrac{mg}{k_3}t_1 \end{cases} \tag{26}$$

Similarly, the speed of the material falling at any time after point D can be obtained.

$$\begin{cases} v_x = v_{Cx}\mathrm{e}^{-\frac{k_3 t}{m}} \\ v_y = \dfrac{mg}{k}\left[\mathrm{e}^{\left(\frac{k_3}{m}+g\right)t} - 1\right] \end{cases} \tag{27}$$

The coordinates of the material after falling at any time t are shown in Equation (28).

$$\begin{cases} L_{xt} = \displaystyle\int_0^{t_1+t} v_x \mathrm{d}t \\ L_{yt} = L_{Dy} - \displaystyle\int_0^t v_y \mathrm{d}t \end{cases} \tag{28}$$

From the above analysis, it can be found that the movement of the material in the drum screen is mainly divided into two stages: 1) M-A-B-C section, the circular motion with the rotation of the drum screen; 2) C-D-M section, leaving the drum screen oblique throwing movement, backward with the drum screen rotation. The tiger nuts mixture repeats the above exercise.

3.3.4 Flow-supporting spiral blade

The cylinder screen needs to transport the material backwards while separating. To improve the backward transport capacity of the drum screen and avoid the accumulation of materials in the screen to affect the screening efficiency, a flow-supporting spiral blade is set inside the drum screen. The rotation direction of the flow-supporting spiral blade is opposite to that of the cylinder screen. The diameter of the flow-supporting spiral blade is equal to the diameter of the cylinder screen, that is, D_1=1.0 m. The pitch of the flow-supporting spiral blade is S_1=0.5 m according to the Agricultural Machinery Design Manual[26] and the actual operation effect.

3.4 Structure design of wind-screen cleaning device

There are light impurities such as broken rhizomes in the extracted tiger nuts after screening by cylinder screen. The suspension speed of broken rhizomes is 6.6-14.5 m/s, and the minimum suspension speed of harvested tiger nuts tubers is 15.8 m/s. Therefore, the air-screen cleaning device is selected in this design to remove the impurities contained in the extracted tiger nuts. The cleaning device is composed of a negative pressure fan, vibrating screen, and other components, as shown in Figure 9.

3.4.1 Design of main parameters of vibrating screen

In the process of wind-screen cleaning, the main function of the vibrating screen is to cooperate with the suction fan to further clean the mixture of tiger nuts screened by the cylinder screening device and remove the broken rhizome. The separation of tiger nut tubers and impurities is completed on the screen surface of the vibrating screen. The vibrating screen transports, disperses, and stratifies the materials through periodic vibration to realize the separation of beans and impurities. The movement of the screen body has an important influence on the movement of the particles on the screen.

The driving mechanism of the vibrating screen adopts the cam linkage mechanism, which can be regarded as the crank linkage mechanism. The kinematics analysis of the mechanism is shown in Figure 10. The rectangular coordinate system *xoy* is established at point *O*, and the motion model of the vibrating screen is established. The line segments *OA* and *AB* represent the crank and connecting rod respectively, *BC* represents the vibrating screen, and *BE* and *CF* represent the front and rear booms of the vibrating screen respectively.

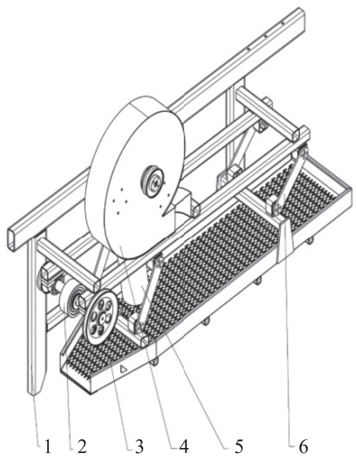

1. Rack 2. Crank rocker mechanism 3. Vibrating screen 4. Fan 5. Fan suction port 6. Connecting rod

Figure 9 Structure diagram of wind-screen cleaning device

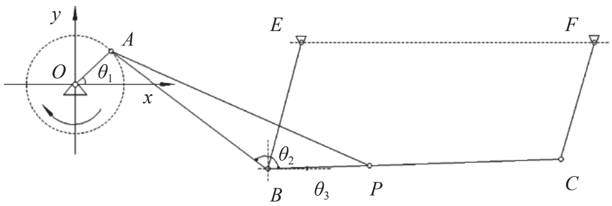

Note: θ_1 is the angle between *OA* and *x* axis, (°); θ_2 is the angle between *AB* and *x* axis, (°); θ_3 is the angle between *BC* and *x* axis, (°).

Figure 10 Motion mechanism diagram of vibrating screen

It is known that the length of *OA* is L_1=10 mm, the length of *AB* is L_2=400 mm, *P* is any point on the screen, the distance to point *B* is L_3, the ordinate y_B of point *B*, and the angular velocity of *OA* rotation.

The closed vector equation $\overrightarrow{OA}+\overrightarrow{AB}+\overrightarrow{BP}=\overrightarrow{OP}$ of the vibrating screen motion mechanism is established, and the motion trend of different points on the screen surface is analyzed. The analytical method is used to convert it into an analytical[32].

$$\begin{cases} \begin{cases} x_A = L_1\cos\theta_1 \\ y_A = L_1\sin\theta_1 \end{cases} \\ \begin{cases} x_B = x_A + L_2\cos\theta_2 \\ y_B = y_A - L_2\sin\theta_2 \end{cases} \\ \begin{cases} x_P = x_B + L_3\cos\theta_3 \\ y_P = y_B + L_3\sin\theta_3 \end{cases} \end{cases} \tag{29}$$

where, x_A is the abscissa of point *A*; y_A is the ordinate of point *A*; x_B is the abscissa of point *B*; y_B is the ordinate of point *B*; x_P is the abscissa of point *P*; y_P is the ordinate of point *P*; θ_1 is the angle between *OA* and *x*-axis, rad; θ_2 is the angle between *AB* and *x*-axis, rad; θ_3 is the angle between *BC* and *x*-axis, rad.

From the second equation of Equation (29), θ_2 can be obtained.

$$\begin{cases} \sin\theta_2 = \dfrac{y_A - y_B}{L_2},\ \dfrac{\pi}{2}\leq\theta_2\leq\dfrac{3\pi}{2} \\ \theta_2 = \arctan\left[\dfrac{y_B - y_A}{L_2^2-(y_A-y_B)^2}\right]+\pi \end{cases} \tag{30}$$

From the third equation of Equation (29), θ_3 can be obtained.

$$\begin{cases} \sin\theta_3 = \dfrac{y_P - y_B}{L_3},\ \dfrac{\pi}{2}\leq\theta_3\leq\dfrac{3\pi}{2} \\ \theta_3 = \arctan\left[\dfrac{y_B - y_P}{L_3^2-(y_P-y_B)^2}\right]+\pi \end{cases} \tag{31}$$

By introducing the results of Equation (30) and (31) into Equation (29), the three-point displacement equations of *A*, *B*, and *P* can be obtained. The first derivative and the second derivative of the displacement equation of each point are obtained respectively, and the velocity and acceleration equations of each point can be obtained.

$$\begin{cases} \begin{cases} \dot{x}_A = -\dot{\theta}_1 L_1\sin\theta_1 \\ \dot{y}_A = \dot{\theta}_1 L_1\cos\theta_1 \end{cases} \\ \begin{cases} \ddot{x}_A = -L_1\left(\dot{\theta}_1^2\cos\theta_1 + \ddot{\theta}_1\sin\theta_1\right) \\ \ddot{y}_A = L_1\left(\ddot{\theta}_1\cos\theta_1 - \theta_1^2\sin\theta_1\right) \end{cases} \end{cases} \tag{32}$$

$$\begin{cases} \begin{cases} \dot{x}_B = \dot{x}_A - \dot{\theta}_2 L_2\sin\theta_2 \\ \dot{y}_B = \dot{y}_A - \dot{\theta}_2 L_2\cos\theta_2 \end{cases} \\ \begin{cases} \ddot{x}_B = \ddot{x}_A - L_2\left(\dot{\theta}_2^2\cos\theta_2 + \ddot{\theta}_2\sin\theta_2\right) \\ \ddot{y}_B = \ddot{y}_A + L_2\left(\ddot{\theta}_2\cos\theta_2 - \theta_2^2\sin\theta_2\right) \end{cases} \end{cases} \tag{33}$$

$$\begin{cases} \begin{cases} \dot{x}_P = \dot{x}_P - \dot{\theta}_3 L_3\sin\theta_3 \\ \dot{y}_P = \dot{y}_P + \dot{\theta}_3 L_3\cos\theta_3 \end{cases} \\ \begin{cases} \ddot{x}_P = \ddot{x}_B - L_3\left(\dot{\theta}_3^2\cos\theta_3 + \ddot{\theta}_3\sin\theta_3\right) \\ \ddot{y}_B = \ddot{y}_B + L_3\left(\ddot{\theta}_3\cos\theta_3 - \theta_3^2\sin\theta_3\right) \end{cases} \end{cases} \tag{34}$$

In summary, the motion trend of each point on the screen surface of the vibrating screen is affected by the structural parameters such as the longest diameter of the cam and the length of the connecting rod. Considering the installation space of the vibrating screen and the matching item of the whole machine, combined with the previous prototype test, the longest diameter of the cam L_1 = 10 mm, the connecting rod L_2 = 400 mm, the length of the vibrating screen frame is 1700 mm, and the inclination angle of the screen surface is 5°.

3.4.2 Screening surface material motion analysis of vibrating screen

According to the analysis of the motion mechanism of the vibrating screen, the vibrating screen does reciprocal motion along the *x*-axis under the action of the crank connecting rod, that is, simple harmonic motion. The movement of the material on the screen mainly has four states: forward slip, backward slip, jump, and relative static. When the material particles move on the screen surface, they are affected by the inertia force, friction force, and gravity of the vibrating screen. To ensure the stratification and forward movement of tiger nuts and rhizome, avoid material accumulation, and affect the screening efficiency, the screen surface is close to the feed end. Point, analyze the movement trend of the material, establish the *xoy* coordinate system with the screen surface as the *x*-axis, and construct the force model of the forward sliding motion of the material particles, as shown in Figure 11.

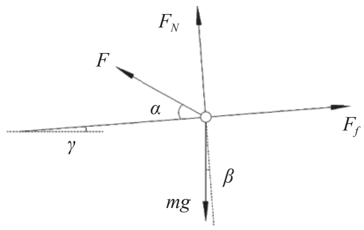

Note: θ_1 is the angle between OA and x axis, (°); θ_2 is the angle between AB and x axis, (°); θ_3 is the angle between BC and x axis, (°).

Figure 11 Force diagram of particle movement on the sieve

As shown in Figure 11, when the particles on the screen slide forward, the friction force is opposite to the sliding direction, and the resultant force of the inertial force and the friction force along the screen surface provides the acceleration for the particles to slide forward[33]. When the acceleration of the vibrating screen $a > 0$, the force of the particles is

$$\begin{cases} F_N = mg\cos\beta - F\sin\alpha \\ F_f = F_N\tan\varphi \\ F_a = ma = F\cos a + mg\sin\beta - F_f \end{cases} \tag{35}$$

where, a is the acceleration of particle sliding, m/s^2; φ is the friction angle between particles and sieve surface, (°).

The inertial force F of the particles on the screen surface is mainly related to the motion state of the vibrating screen, and its expression is Equation (36).

$$F = mA\omega^2\sin(\omega t) \tag{36}$$

where, ω is the cam angular velocity, rad/s; A is the amplitude of vibrating screen, m.

From the analysis of Equation (36), when the support force F_N>0, the condition of forward sliding motion is

$$\begin{cases} F_N > 0 \\ F_a > 0 \end{cases} \tag{37}$$

From Equations (35)-(37), Equation (38) can be obtained:

$$\begin{cases} F_N = mg\cos\beta - mA\omega^2\sin(\omega t)\sin\alpha > 0 \\ F_a = ma = mA\omega^2\sin(\omega t)(\cos\alpha + \sin\alpha\tan\varphi) - \\ \quad mg(\sin\beta - \cos\beta\tan\varphi) > 0 \end{cases} \tag{38}$$

Similarly, the conditions can be determined for the particles on the screen to slide forward when the acceleration of the vibrating screen $a < 0$ as Equation (39).

$$\begin{cases} F_N = mg\cos\beta + mA\omega^2\sin(\omega t)\sin\alpha > 0 \\ F_a = ma = mg(\cos\beta\tan\varphi + \sin\beta) - \\ \quad mA\omega^2\sin(\omega t)(\sin\alpha\tan\varphi + \cos\beta) > 0 \end{cases} \tag{39}$$

Through Equation (39), the particle forward slip acceleration can be obtained.

$$a = A\omega^2\sin(\omega t)(\cos a + \sin\alpha\tan\varphi) - mg(\sin\beta - \cos\beta\tan\varphi) \tag{40}$$

The forward slip velocity of particles can be obtained.

$$v = -A\omega\cos(\omega t)(\cos a + \cos a\tan\varphi) - mgt\tan\varphi \tag{41}$$

When the particle falls into the screen surface for the first time, the velocity along the direction of the sieve surface is 0, and the moving distance X of the particle along the screen surface after t_1 time can be obtained.

$$X = \frac{1}{2}at^2 = \frac{1}{2}t^2\begin{bmatrix} A\omega^2\sin(\omega t)(\cos a + \sin a\tan\varphi) \\ -mg(\sin\beta - \cos\beta\tan\varphi) \end{bmatrix} \tag{42}$$

According to Equation (42), the forward sliding distance of particles on the screen is affected by the cam radius and rotational speed. When the cam radius increases and the rotational speed increases, the forward sliding acceleration of particles increases, the horizontal moving distance increases, and the material migration speed increases, which is conducive to the dispersion of materials on the screen surface, avoiding accumulation in the screen body and improving the cleaning efficiency.

3.4.3 Determination of fan parameters

The main function of the fan is to remove the light impurities such as broken rhizomes in the mixture of tiger nuts which is dispersed and layered by the vibrating screen and transported to the suction port. In the preliminary test, the suspension speed of broken rhizome was 7.0-14.1 m/s, and the suspension speed of tiger nuts was not less than 16.0 m/s. According to the different suspension speed of impurities and tiger nuts, the average airflow speed of the suction port of the fan was set to 14.8 m/s, and the calculation formula of the air volume V (m^3/s) of the air separation airflow was[26]

$$V = \frac{\lambda Q}{\mu\rho} \tag{43}$$

where, Q is the quality of feeding material, kg/s; λ is the proportion of impurities in the feed material, %; ρ is the air density, kg/m^3; u is the mixed concentration ratio of the airflow carrying impurities, about 0.2-0.3.

The height H_C (m) of the suction port from the vibrating screen needs to meet the needs of the cleaning gas flow rate and the air flow rate, which can be expressed as Equation (44).

$$H_C = \frac{V}{Bv} \tag{44}$$

where, V is the cleaning gas flow rate, m^3/s; B is the width of the suction port, m; v is the airflow velocity of the suction port, m/s.

According to the above, the maximum speed of the fan n= 1050 r/min is calculated, and the actual operation fan speed is determined to be 1050 r/min.

3.5 Simulation of screening process of cylinder screening device

3.5.1 Simulation parameter setting and model construction

With the development of computer technology, the discrete element method (DEM) has become a powerful tool for studying the particle screening due to its unique advantages in simulating the macroscopic flow and microscopic interaction of particle systems[20,21,33]. To validate the structural rationality of the cylinder screening device, EDEM 2022 (DEM Solutions, Edinburgh, UK), a commercial software package based on DEM, was employed to simulate the screening process. As shown in Figure 12, the spherical particles with a diameter of 1 mm are generated in EDEM to represent the soil particle simulation model. The tuber is constructed by SolidWorks 2021 to construct a three-dimensional model, which is saved as .stl, and imported into EDEM to be filled with particles. The stem is composed of spherical particles with a diameter of 1 mm and a length range of 10-50 mm, which is consistent with the harvest time. Because in the screening process, the focus is on the simulation and analysis of particle migration and screening process, and the soil in the planting area is sandy loam, the soil is loose and the water content is low, so the Hertz-Mindlin (no slip) contact model is selected in the numerical simulation process. The intrinsic parameters and contact parameters of each material are obtained through previous experiments and related literatures[21,34,35], as listed in Tables 2 and 3.

Figure 12 Material simulation model

Table 2 Material intrinsic parameters

Material	Density/kg·m^{-3}	Poisson's ratio	Young's modulus/Pa
Soil	1638	0.3	1.15×10^{7}
Tuber	1089	0.41	3.34×10^{7}
Stem	470	0.4	1.72×10^{6}
Steel	7850	0.28	7.00×10^{10}

Table 3 Material contact parameters

Material	Restitution coefficient	Static friction coefficient	Rolling friction coefficient
Soil and Soil	0.40	0.50	0.30
Soil and Tuber	0.50	0.50	0.30
Soil and Stem	0.48	0.05	0.32
Soil and Steel	0.40	0.43	0.35
Tuber and Tuber	0.43	0.48	0.05
Tuber and Stem	0.35	0.05	0.10
Tuber and Steel	0.45	0.41	0.06
Stem and Stem	0.60	0.33	0.14
Stem and Steel	0.31	0.41	0.01

Inventor 2021 is used to construct a three-dimensional model of the cylinder screening device, which is saved in STEP format and imported into EDEM 2022 software. To improve the simulation efficiency, the model is simplified into two parts: cylinder screening and screw conveyor. The particle factory is set inside the drum screen, and the simulation parameters are set based on the feeding amount of the conveying and sand removal device and the proportion of each component. The total material generation rate is 25 kg/s, of which soil accounts for 91.9%, tubers account for 3.4%, and stems account for 4.7%. The particle generation time is set to 5 s. After the particles are completely generated, the particle factory is removed, and the file is saved. The initial simulation time is set to 0 s, and the cylinder speed is determined as 25 r/min according to the analysis in Section 2.3.3. The cylinder screening process is simulated. The simulation time is set to 10 s, the time step is set to 20%, and the data storage time is set to 0.1 s.

3.5.2 Cylinder screening process analysis

To facilitate the analysis of the separation of sand and soil in the cylinder screening process, the soil particles are marked with different colors according to the speed in the EDEM post-processing module. From large to small, they are red, green, and blue, respectively. The black arrow represents the rotation of the drum screen. At the same time, in the circumferential of the drum screen, the bottom of the cylinder screen is taken as the starting point, and it is divided into four blocks along the circumference according to the angle, which are 0°-90°, 90°-180°, 180°-270°, and 270°-360°(0°) (Figure 13a). In addition, to clarify the movement of soil particles during the screening process, seven tracer particles are randomly selected to obtain the trajectory during the screening process (Figure 13b).

It can be seen from Figure 13a that during the screening process, the soil particles are circularly moving in the counterclockwise direction at the bottom of the cylinder screen, and the main soil particle separation area is concentrated between the inner and outer screen layers. Especially in the 0°-90° area, due to the centrifugal force, most of the particles can pass through the screen and be discharged smoothly, which is the main discharge area. Some particles are lifted to the 90-180° area with the cylinder screen and fall back to the bottom under the action of gravity, which is consistent with the theoretical analysis results in Section 2.3.3.

Combined with the trajectory of soil particles in Figure 13b, a few particles pass through the screen directly when entering the screening device, while most of the particles are pushed axially by the spiral conveyor and the flow-assisted spiral blade. On the one hand, they move circularly with the cylinder screen; on the other hand, they move along the axial direction, and then pass through the screen hole to discharge out of the machine. The separation area of soil particles is mainly concentrated in the front end of the cylinder screen, and the separation effect is more significant.

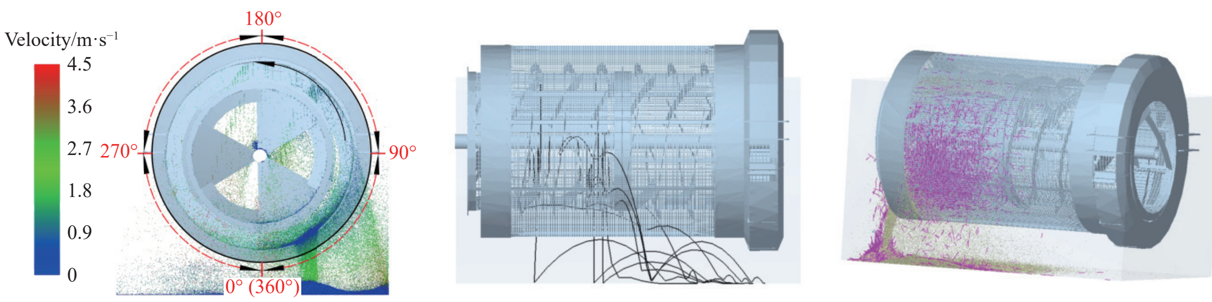

Figure 13 Dynamic simulation of cylinder screening process

It can be seen from Figure 13c that in the process of cylinder screening, the migration area of rhizome mainly exists in the inner side of the inner cylinder screen. On the one hand, they move circularly with the cylinder screen, and on the other hand, they move along the axial direction under the action of the screw conveyor until they are discharged from the outside of the machine. In addition, some broken rhizomes will enter the outer screen through the inner screen, migrate with the soil particles, and finally be discharged through the outer screen. The migration and separation effects of the materials in the screen are ideal, and the role of the spiral conveyor and the guide vane has also been fully utilized. The screen design is reasonable, which not only ensures the effective separation of rhizome and soil, but also improves the efficiency and accuracy of screening.

4 Field experiment

4.1 Test conditions

The experiment was carried out in October 2023 in the planting test base of tiger nuts in the 54th Regiment of the Third Division of Xinjiang Production and Construction Corps. As shown in Figure 14, the variety of tiger nut was Zhongyousha 1. The row spacing of tiger nuts in the test site was between 20-30 cm, and the plant spacing was between 4-7 cm. The aboveground stems and leaves were harvested before the experiment, and the stubble height was 7-10 cm. The water content of tiger nuts in the test site was 26%, and the water content of rhizome was 20.2%.

Figure 14 Growth situation of tiger nuts

4.2 Test methods and indicators

According to the China Standards[36,37], the four working performance indices of net rate, impurity rate, working efficiency, and digging depth were measured respectively in the test of 4USQ-1600 traction tiger nut combine harvester (Figure 15).

Figure 15 Tiger nut harvester operation site

Before the test, the well-growing blocks of tiger nuts were selected, and the test area was delimited. The test area was 30 m long, and 10 m was reserved before and after each as the preparation area, and the width was eight times the width of the operation. In the test area, five typical areas were selected as the performance test area, each of which was 3 m long, and the width was the operation width. Before the operation, the natural fruit drop in the test area was picked out, and a region was selected to delineate three 1 m×1 m areas to predict the yield of tiger nuts. Before the operation, five points were divided as test points to determine the excavation depth of each test point, which was calculated according to Equation (45). At the same time, the productivity of pure working hours, that is, operating efficiency, was calculated according to Equation (46). After the operation, all the missing and falling tiger nuts in the process of excavation, sand removal, threshing, cleaning, and separation were collected in the test area, and the mass was weighed. The loss rate was calculated according to Equation (47). All the tiger nuts and impurities in the collection box were separated, and the mass was weighed respectively. The impurity rate was calculated according to Equation (48). Each group of tests was repeated three times.

$$H = \frac{\Sigma h_i}{5} \tag{45}$$

where, H is the depth of the digging, cm; h_i is the digging depth of each test point, cm.

$$E = \frac{Q}{T} \tag{46}$$

where, E is work efficiency, hm^2/h; Q is the amount of work in the assessment time, hm^2; T is the assessment time, h.

$$Y_1 = \frac{m_1 + m_2}{m} \times 100\% \tag{47}$$

$$Y_2 = \frac{m_4}{m_3 + m_4} \times 100\% \tag{48}$$

where, Y_1 is the loss rate, %; Y_2 is the impurity rate, %; m is the total mass of tiger nuts, and $m = m_1 + m_2 + m_3$, kg; m_1 is the quality of miss-digging tiger nuts, kg; m_2 is the quality of the fallen tiger nuts, kg; m_3 is the quality of tiger nuts in the collection box, kg; m_4 is the quality of the impurity, kg.

4.3 Test results

Referring to the China Standards[36-37], combined with the growth environment and agronomic requirements of tiger nuts, the total loss rate of tiger nut combine harvester is required to be ≤5%, the impurity rate is ≤10%, and the excavation depth is ≥10 cm. According to the operation specification and test standard, the performance index of the machine is measured. The whole machine and each device run stably during the operation process. The digging device, conveying and sand removal device, drum screening device, and cleaning device work normally. The average loss rate during the harvest process is 4.88%, and the average impurity rate (excluding stones) is 7.52%. The average excavation depth is ≥12.5 cm, and the operation effect and harvest efficiency reach the expected value, which meets the operation requirements of the tiger nut combine harvester.

5 Discussion

Problems such as low harvesting efficiency, high impurity rates, and significant losses persist during the tiger nut harvesting process[8,14,21]. In this study, the operation mode of "sand removal first and then separating" was proposed based on the fact that more than 95% of the soil mass in the tiger nut mixture was sand. A tiger nut combine harvester was designed, integrating vibration excavation device, conveying and sand removal device, double-layer drum screening device, and air-screen cleaning device (Figure 1). Compared with the "separation concurrent with sand removal" mode, the high soil-containing mixture enters the separation device at the same time, which increases the load and power consumption of the separation device. The scheme proposed in this paper can remove 88.92% of the sand before the mixture of tiger nuts and roots enters the threshing drum[28], so as to reduce the power consumption of the whole machine.

In the actual field operation, the harvester passed the operation mode of "sand removal first and then separating", and the average loss rate and impurity rate were 4.88% and 7.52%, respectively. In contrast, Reference [21] pointed out that if the soil-containing mixture directly enters the screening device, the impurity rate will surge to 25.55%. This difference can be attributed to the fact that the influx of a large amount of soil increases the dynamic load per unit area of the sieve surface, resulting in a decrease in screening efficiency. Under the extrusion of soil, more grass masses were forced to pass through the inner sieve into the outer sieve, and finally discharged with the tiger nuts, resulting in a sharp increase in impurity rate. The scheme adopted in this paper removes 88.92% of the soil in the conveying stage, reduces the feeding amount of the separation device, and ensures the effective working area. This conclusion is consistent with the result of Qu et al.[8] that the loss rate and impurity rate of the air screen system are lower after the first dumping of the chain lifting device. It is further confirmed that reducing the load of the separation device is the key to balancing the loss rate and impurity rate for the high-sand harvest object of tiger nuts.

The impurity rate of tubers obtained in the harvest stage was 7.52%, and 88.92% of soil removal was achieved in the conveying sand removal stage. This reduces the time and water consumption required for separation and cleaning before subsequent processing. Under the operation mode of "sand removal first and then separating" the breaking rates of excavation and transportation sand removal links are 2.62% and 1.71% respectively[16,28]. This effectively ensures the quality of tiger nut tubers and prevents oxidation during subsequent storage and processing, thereby preserving the commercial value of the crop.

6 Conclusions

1) Aiming at the problems of high impurity rate and high loss rate in the harvesting process of tiger nuts, a new harvesting operation mode of "sand removal first and then separating" was proposed, and a traction tiger nuts combine harvester was designed, which can realize the integrated operation of excavation, conveying and sand removal and threshing separation, improve the harvesting efficiency and quality, and make up for the deficiency of mechanized harvesting of tiger nuts in China.

2) Through the calculation of mining conditions, power consumption, etc., it was determined that the rotary tillage mining device is a combined vibration mining, and the transmission mode is chain drive. Then combined with the previous research on the conveying sand removal device, the design of the conveying sand removal device was completed. The kinetic and kinematic equations of the material in the process of double-layer drum screening were established, and the diameter and size of the drum screen were determined. The EDEM discrete element simulation model was constructed, and the motion state and screening principle of tiger nuts mixture in the double-layer drum screen were analyzed. The structural design and working parameters of the double-layer drum screening device were determined. Through the dynamic and kinematic analysis of the vibrating screen body and the screen surface particles, the structural working parameters of the vibrating screen and the fan were determined.

3) Field experiments showed that the average loss rate of the whole machine during the harvest process was 4.88%, the average impurity rate (excluding gravel content) was 7.52%, and the excavation depth was ≥12.5 cm. During the test, the whole machine was in good working condition, and all indicators met the technical requirements of the domestic tiger nuts harvester.

Acknowledgements

This work was financially supported by the Xinjiang Production and Construction Corps Youth Science Fund Program (Grant No. 2024DB016), Xinjiang Production and Construction Corps Guiding Science and Technology Program (Grant No. 2024ZD036), and the Science and Technology Research Program of Shihezi University (Grant No. KJGG202404).

[References]

[1] Ezeh O, Gordon M H, Niranjan K. Tiger nut oil (*Cyperus esculentus* L.): A review of its composition and physico-chemical properties. European Journal of Lipid Science & Technology, 2014; 116(7): 783–794.

[2] Bado S, Bazongo P, Son G, Kyaw M T, Forster B P, Nielen S, et al. Physicochemical characteristics and composition of three morphotypes of *Cyperus esculentus* tubers and tuber oils. Journal of Analytical Methods in Chemistry, 2015; 2015(1): 673547.

[3] Zhang Y, Sun S. Tiger nut (*Cyperus esculentus* L.) oil: A review of bioactive compounds, extraction technologies, potential hazards and applications. Food Chemistry: X, 2023; 19: 100868.

[4] Nwosu L C, Edo G I, Ozgor E. The phytochemical, proximate, pharmacological, GC-MS analysis of *Cyperus esculentus* (Tiger nut): A fully validated approach in health, food and nutrition. Food Bioscience, 2022; 46: 101551.

[5] Edo G I, Ugbune U, Ezekiel G O, Onoharigho F O, Agbo J J. *Cyperus esculentus* (tiger nut): its application in agriculture, food, health and nutrition: A review. Vegetos, 2023; 37: 757–766.

[6] Nina G C, Goncharov A, Batishcheva N, Vlasov S, Okuskhanova E, Císarová M, et al. Proximate, mineral and functional properties of tiger nut flour extracted from different tiger nuts cultivars. Journal of Microbiology, Biotechnology and Food Sciences, 2019; 9(3): 653–656.

[7] Li J, Liu W L, Zhang L, Wang X Y, Zhang Y H. Design and experiment on harvesting equipment of Cyperus bean. Agricultural Engineering, 2022; 12(4): 36–39. (in Chinese)

[8] Qu Z, Han M, Lv Y, Zhou Z, Lv Z, Wang W, He X. Design and test of a crawler-type tiger-nut combine harvester. Agriculture, 2023; 13(2): 277.

[9] Dong R J, Xiao J, Liu W L, Guo W H, Wang X Y, Liu F. Design and experiment of traction *Cyperus esculentus* harvester. Journal of Chinese Agricultural Mechanization, 2024; 45(1): 21–27. (in Chinese)

[10] Liu W L, Yan H Y, Liu F, Jiang C Y, Zhang L, Wang X Y. Design and experiment of compound screening *Cyperus esculentus* harvester. Agricultural Engineering, 2023; 13(2): 88–94.

[11] Liu W L, Kong L Y, Jiang C Y, Wang X Y, Zhang L. Design of the tiger nut harvester. Agricultural Development & Equipment, 2023; 13(2): 88–94. (in Chinese)

[12] Wang H C, Zhao W Y, Sun W, Zhang H, Liu X L, Li H. Research progress on the technology and equipment for potato mechanized harvesting. Transactions of the CSAE, 2023; 39(14): 1–22. (in Chinese)

[13] Zhao Z, Wang D W, He X N, Sheng S Q, Shen S L, Xia C, et al. Design and test of the anti-rotation throwing device of the *Cyperus edulis* combine harvester. Journal of Agricultural Mechanization Research, 2023; 45(7): 65–70. (in Chinese)

[14] He X N, Zhang X J, Zhao Z, Shang S Q, Wang D W, Yang S. Design and optimization tests of reverse spin-throwing *Cyperus edulis* starting device. Transactions of the CSAM, 2022; 53(5): 34–43. (in Chinese)

[15] Zhang X J, Dai F, Shi R J, Zhao W Y, Ma H J, Zhao X P. Design and experiment of vibrating separating rhizome harvesting machine for Chinese medicinal materials. Agricultural Research in the Arid Areas, 2024; 42(3): 264–275. (in Chinese)

[16] Pei M H, An S G, Chen S, Qi J T, Li Y P. Analysis and experimentation of the crushing and separation process of the root-sand complex of harvested and excavated *Cyperus esculentus* L. in deserts. Engenharia Agrícola, 2023; 43(3): e20220121.

[17] Wang F A, Wen B, Xie X H, Xie K T, Guo S W, Zhang S W, et al. Operation mechanism analysis and parameter optimization of conveying and separating device of *Panax notoginseng* harvester. Transactions of the CSAM, 2023; 54(S1): 201–211, 259. (in Chinese)

[18] Zhao Z, He X N, Wang D W, Sheng S Q, Xu N, Zhu H, et al. Design and test of the anti-rotation throwing device of the *Cyperus Edulis* combine harvester. Journal of Agricultural Mechanization Research, 2023; 45(8): 172–176. (in Chinese)

[19] Xin L, Liang J. A dynamic analysis on the potato conveying and separation system considering the acting force of a material. Transactions of FAMENA, 2019; 43(SI-1): 35–42.

[20] Chen M, Liu X, Hu P, Zhai X, Han Z, Shi Y, et al. Study on rotor vibration potato-soil separation device for potato harvester using DEM-MBD coupling simulation. Computers and Electronics in Agriculture, 2024; 218: 108638.

[21] Zhang S W, Zhang R Y, Cao Q Q, Zhang Y, Fu J, Yuan H F. Design and experiment of double-deck roller sieve type fruit impurity separation device for tiger nut harvester. Transactions of the CSAM, 2023; 54(3):

148–157. (in Chinese)

[22] Pei M H. Design and research of vibratory excavation apparatus for *Cyperus esculentus* L. Master dissertation. Shihezi University, Shihezi, 2022; 78p. (in Chinese)

[23] Awuah E, Zhou J, Liang Z, Aikins K A, Gbenontin B V, Mecha P, et al. Parametric analysis and numerical optimisation of Jerusalem artichoke vibrating digging shovel using discrete element method. Soil & Tillage Research, 2022; 219: 105344.

[24] Wang F A, Ni C, Zhang Z G, Xu H W, Xie K T, Wang B Y. Analysis and experiment on drag reduction characteristics of digging shovel of panax notoginseng harvester. Transactions of the CSAM, 2024; 55(7): 179–190, 199. (in Chinese)

[25] Zheng Y Y, Guo D, Wang Z Z, Yang R B. Improved design and experiment of potato digging shovel. Journal of Agricultural Mechanization Research, 2021; 43(3): 137–140. (in Chinese)

[26] First Ministry of Machinery Industry, Machinery Research Institute, Agricultural Machinery Design Manual. Volume 1. Machinery Industry Press, 1988.

[27] Wei G J, Qi B, Jiao W, Shi S, Jian S C. Design and experiment of mechanical forced fertilizing device for paddy field. Transactions of the CSAM, 2020; 51(S1): 154–164. (in Chinese)

[28] Qi J T, Gao J P, Chen S, Chen W H, Yang L Y, Meng H W, et al. Parameter optimization of a conveying and separating device based on a five-stage screw and vibrating screen for tiger nut harvesters. Agriculture, 2024; 14(5): 682.

[29] Hu Y G, Li Y G, Li J G, Lu H Y, Xiao H R. Design and experiment of equant-diameter roller screening machine for fresh tea leaves. Transactions of the CSAM, 2015; 46(S1): 116–121. (in Chinese)

[30] Yuan J C, Yang J, Wan X Y, Liao Y T, Liao Q X. Design and experiment of cylinder sieve type re-cleaning device for rape combine harvester. Transactions of the CSAM, 2022; 53(9): 99–108. (in Chinese)

[31] Wang S S, Chen P, Lu M Q, Geng L X, Ji J T, Yang F. Design and experiment of separation and cleaning device for Chinese cabbage seeds harvester. Transactions of the CSAM, 2020; 51(S2): 181–190. (in Chinese)

[32] Zhang X J, Zhang Y H, Shi Z L, Ma S T, Huang S, Cheng J P. Optimization and experiment of oil sunflower combined harvester cleaning device. Transactions of the CSAM, 2022; 53(8): 103–113. (in Chinese)

[33] Li H, Mu G, Zhang H, Wu H, Liu F, Sun Z, et al. Design and testing of a mechanized brush-screen cooperative vibration harvester for mudflat-buried shellfish based on the discrete element method. Frontiers in Marine Science, 2023; 10: 1134888.

[34] Qi J T, Chen S R, Yang L Y, An S G, Meng H W, Kan Z. Calibration of contact parameters of sandy soil for planting tiger nut based on non-linear tools. Scientific Reports, 2024; 14(1): 13895.

[35] Qi J T, An S G, Kan Z, Meng H W, Li Y P, Zhao X Y. Discrete element-based calibration of simulation parameters of Cyperus esculentus L. (tiger nut) planted in sandy soil. Journal of Food Processing and Preservation, 2021; 45(7): e15631.

[36] GB/T 5262-2008. General provisions for the determination methods of agricultural machinery test conditions. China Standards Press, 2008. Available: https://www.bzchaxun.com/view/6044141003000000.html. Accessed on [2024-10-19]. (in Chinese)

[37] DG/T 286-2023. Cyperus esculentus harvester. Ministry of Agriculture and Rural Affairs of China, 2023. Available: http://www. moa. gov. cn/zxfile/reader?file=http://www.moa.gov.cn/govpublic/NYJXHGLS/202302/P020230206299208628311.rar. Accessed on [2024-10-19]. (in Chinese)